JOURNAL OF Materials CHEMISTRY

Poly[(silylene)diacetylene]/fine metal oxide powder dispersions: use as precursors to silicon-based composite ceramics

Robert J. P. Corriu, Philippe Gerbier,* Christian Guérin* and Bernard Henner

U.M.R. 5637 Chimie Moléculaire et Organisation du Solide, Université Montpellier II, Sciences et Techniques du Languedoc, Place Eugène Bataillon - Case 007, 34095 Montpellier cedex 5, France. E-mail: gerbier@crit.univ-montp2.fr

Received 7th April 2000, Accepted 23rd June 2000
Published on the Web 4th August 2000

A synthetic route to silicon-based composite ceramics that employs organosilicon polymer/metal oxide precursors is described. The precursor materials were obtained by dispersing metal oxides in the poly[(silylene)diacetylenes] **1**. Subsequent pyrolysis of the dispersions above 1400 °C under various experimental conditions afforded β-SiC-based metal carbides and metal nitrides, metal silicides and Si_3N_4-based composites of defined compositions, in high ceramic yields. Under atmospheres of argon or of nitrogen, the precursor-to-ceramic conversion involved two critical transformations: i) the thermal cross-linking of **1** leading to an irreversible encapsulation of the oxide particle inside the polymeric matrix and ii) the carbothermal reduction of the oxide constituents by the carbon resulting from the degradation of polymer **1** to produce either the final carbide or the final nitride under the pyrolysis conditions. Moreover, it is shown that the encapsulation of the oxide particles inside a reactive matrix led to the formation of particle-tailored micro-scale reactors in which the reduction process took place with high efficiency.

1. Introduction

Because of their high melting points, hardness and chemical resistance at high temperatures, metal carbides and nitrides are two of the most important families of engineering ceramics.[1] As a consequence, formation of novel ceramic materials from polymers consisting of a structural element which is desired in the final product has attracted much attention.[2–17] This chemical route had proved to be superior to the conventional powder technology because of the high purity of its precursor materials, the lower processing temperatures and its versatility in plastic shaping technologies.[5,18] Moreover preceramic polymers have been successfully used either as powdered ceramic binders[19,20] or as reactants toward embedded metal or metal oxide particles.[3,21–27] The latter examples had proved to be excellent alternative routes for the synthesis of composite ceramics which are known to exhibit significantly improved mechanical properties (hardness, toughness, sinterability) when compared to the isolated phases, allowing their potential use in cutting tools, abrasives or high-temperature structural applications.[25–33]

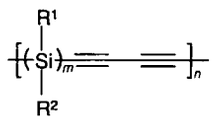

1a: $m = 1$, $R^1 = R^2 = CH_3$
1b: $m = 2$, $R^1 = R^2 = CH_3$
1c: $m = 1$, $R^1 = R^2 = C_6H_5$

In previous works,[34–37] we described a novel class of organosilicon linear polymers incorporating diacetylenic units such as poly[(silylene)diacetylenes] **1**. **1** are organosoluble linear polymers which are synthesized in high yields by polycondensation of a dichlorosilane with 1,4-dilithio-butadiyne in THF (Scheme 1).[37] When pyrolyzed at 1400 °C under an argon flow, **1** led to black residues in high char yields with compositions depending upon the nature of the substituents at the silicon atoms (Table 1); all the silicon present in the organosilyl groups of the starting polymers is found in the ceramic as SiC. On the other hand, when pyrolyzed under ammonia, they led to Si_3N_4 whiskers.[35] The exothermic cross-linking of the diacetylenic units[38,39] which occurs in the solid state at 200 °C overcomes depolymerization processes and explains the high ceramic yield obtained with such polymers.[36,40]

In earlier preliminary communications,[21,23] we reported that β-SiC/metal carbide (or nitride) can be obtained in high yields by means of a potentially general polymer-precursor route[22] using dispersions of a metal oxide in polymers **1**. The metal oxide : **1** ratio was adjusted in such a way that the carbothermal consumption of the excess of carbon by the oxide provides pure β-SiC/metal carbide (or nitride) ceramics of defined compositions. Quite recently, we have demonstrated that β-SiC/MC (M = Ti, Nb and Ta) nanocomposite ceramics are obtained from the pyrolysis under argon of precursors consisting of interpenetrating networks of polymer **1a** and of polymeric metal oxide generated by an *in situ* precipitation of the corresponding metal alkoxide.[41]

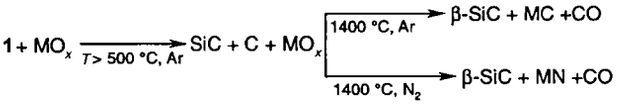

We report herein full details of our work and the potential of this method to prepare a wide range of silicon-based ceramic composite materials.

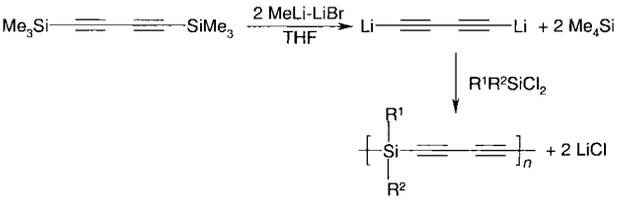

Scheme 1 Synthesis of polymers **1**.

DOI: 10.1039/b002788j

Table 1 Pyrolysis of poly[(silylene)diacetylenes] under argon: ceramic yields and chemical composition of the residues

Polymer	Ceramic yield (%)	Composition[a]	Stoichiometry of the ceramic	Free C (%)	Si conservation (%)[b]
1a	84	$Si_{1.00}C_{5.11}$	SiC–4C	54.5	97
1b	72	$Si_{1.00}C_{3.21}$	2(SiC)–4C	37.5	90
1c	83	$Si_{1.00}C_{12.89}$	SiC–12C	78.3	94

[a]Based on elemental analysis. [b]Based on the ratio Si previously present in the polymer/Si recovered in the final ceramic.

Table 2 Characteristics of the metal oxides

Metal oxide	Origin	Purity (%)	Type and/or grain size
Al_2O_3	Rhône-Poulenc	99	75–180 μm
SiO_2	Rhône-Poulenc	99	aerogel, < 1 μm
TiO_2	Prolabo	99	anatase, < 5 μm
V_2O_5	Aldrich	98	75–180 μm
Co_3O_4	Aldrich	72–73[a]	< 1 μm
NiO	Aldrich	99	black, ± 5 μm
Nb_2O_5	Aldrich	99.5	< 45 μm
MoO_3	Aldrich	99+	10–20 μm
$PdO{\cdot}xH_2O$[b]	Aldrich	76[a]	—
Ta_2O_5	Interchim	99	< 45 μm
WO_3	Aldrich	99+	≈ 20 μm
$PtO_2{\cdot}xH_2O$[b]	Aldrich	80[a]	—

[a]Metal content. [b]The oxides are dehydrated by heating at 100 °C under 1 mmHg for 24 h prior to be used.

2. Experimental

2.1. General

In the text, dispersions of type **A** will refer to precursors in which the starting metal oxide leads to a metal carbide upon pyrolysis under an inert atmosphere, whereas in dispersions of type **B**, the metal oxide leads to a metal silicide.

The characteristics of the metal oxides used in this work are given in Table 2. THF was distilled over CaH_2 prior to use. The argon or nitrogen (ultrapure grade) were purchased from L'Air Liquide and used without further purification. Poly[(silylene)-diacetylenes] **1a–c** were prepared according to the procedure published previously.[37] The ammonia was purified through columns filled with KOH pellets and silica gel respectively.

2.2. Instrumentation

All the pyrolyses were performed in a Carbolite alumina tube furnace fitted with taps to allow connection to a vacuum line. Powder X-ray diffraction (XRD) patterns were recorded on a Philips diffractometer using Cu-Kα radiation. Transmission electron microscopy (TEM) coupled with energy dispersive analysis of X-rays (EDX) was carried out on a Philips CM 20 microscope operating at 200 kV equipped with a TRACOR microprobe. Powder specimens were suspended in ethanol and spread onto a copper grid covered with an amorphous carbon film. Thermal analyses were carried out with a Netzsch STA 409 thermogravimetric analyzer coupled to a Balzers QMG 421 mass spectrometer. Thermogravimetric analyses (TGA) were recorded in the range 20–1400 °C under the desired gas flow (60 mL min^{-1}) at a heating rate of 10 °C min^{-1}. Differential scanning calorimetric (DSC) experiments were conducted on a Mettler 30 instrument. IR spectra were taken on a Perkin Elmer 1600 FT either in KBr pellets or in nujol mulls. N_2 adsorption–desorption isotherms (BET method) were measured on a Micromeritics Gemini apparatus. Elemental analyses were performed at the Service Central de Microanalyse of the CNRS, Vernaison, France.

2.3. Preparation of metal oxide/polymer dispersions

In a typical process, appropriate quantities of the polymer **1** and finely divided metal oxide (Tables 3–6) were mixed in THF under ultrasound for 0.5 h. Then, the mixture was left stirring and the solvent was removed under reduced pressure to yield beige solids.

Table 3 SiC/metal carbide precursor preparation (dispersions of type **A**, pyrolysis under argon)

Polymer	Metal oxide	Polymer weight/g (equiv.)	Metal oxide weight/g (equiv.)	Si : M : C ratio
1a	TiO_2	1.00 (3)	1.00 (4)	3 : 4 : 15
1b	TiO_2	1.37 (3)	1.00 (2)	6 : 2 : 12
1c	TiO_2	0.72 (1)	1.00 (4)	1 : 4 : 13
1a	ZrO_2	0.66 (3)	1.00 (4)	3 : 4 : 15
1a	HfO_2	0.39 (3)	1.00 (4)	3 : 4 : 15
1a	V_2O_5	0.95 (13)	1.00 (8)	13 : 16 : 65
1a	Nb_2O_5	0.70 (7)	1.00 (4)	7 : 8 : 35
1a	Ta_2O_5	0.42 (7)	1.00 (4)	7 : 8 : 35
1a	MoO_3	0.65 (7)	1.00 (8)	7 : 8 : 35
1a	WO_3	0.46 (1)	1.00 (1)	1 : 1 : 5

Table 4 SiC/metal silicide precursor preparation (dispersion type **B**, pyrolysis under argon)

Polymer	Metal oxide	Polymer weight/g (equiv.)	Metal oxide weight/g (equiv.)	Si : M : C ratio
1a	Co_3O_4	1.32 (3)	1.00 (1)	3 : 3 : 15
1a	NiO	0.71 (1)	1.00 (2)	1 : 2 : 5
1a	PdO	0.22 (1)	1.00 (4)	1 : 4 : 5
1a	PtO_2	0.23 (1)	1.00 (2)	1 : 2 : 5

Table 5 SiC/metal nitride precursor preparation (pyrolysis under nitrogen)

Polymer	Metal oxide	Polymer weight/g (equiv.)	Metal oxide weight/g (equiv.)	Si : M : C ratio
1a	TiO_2	0.67 (1)	1.00 (2)	1 : 2 : 5
1a	ZrO_2	0.44 (1)	1.00 (2)	1 : 2 : 5
1a	HfO_2	0.26 (1)	1.00 (2)	1 : 2 : 5
1a	V_2O_5	0.73 (5)	1.00 (4)	5 : 8 : 25
1a	Nb_2O_5	0.50 (5)	1.00 (4)	5 : 8 : 25
1a	Al_2O_3	1.40 (3)	1.00 (4)	3 : 8 : 15
1a	SiO_2	0.88 (1)	1.00 (2)	3 : 0 : 5

Table 6 Si_3N_4-based ceramic precursor preparation (pyrolysis under ammonia)

Polymer	Metal oxide	Polymer weight/g (equiv.)	Metal oxide weight/g (equiv.)	Si : M : C ratio
1a	TiO_2	0.67 (1)	1.00 (2)	1 : 2 : 5
1a	ZrO_2	0.44 (1)	1.00 (2)	1 : 2 : 5
1a	HfO_2	0.26 (1)	1.00 (2)	1 : 2 : 5
1a	Nb_2O_5	0.50 (5)	1.00 (4)	5 : 8 : 25
1a	Ta_2O_5	0.30 (5)	1.00 (4)	5 : 8 : 25
1a	Al_2O_3	1.40 (3)	1.00 (4)	3 : 8 : 15

2.4. Pyrolysis

The pyrolyses were carried out on weighed samples (0.1 to 1 g) of polymer/metal oxide dispersions placed into alumina crucibles, which were heated in an alumina tube fitted with glass taps to allow connection to a vacuum line. After 3 gas

Table 7 SiC/metal carbide pyrolysis products (type **A**, under argon)

Polymer (equiv.)	Metal oxide (equiv.)	Ceramic yield (%)[a]	Stoichiometry of the ceramic[b] (MC [%])
1a (3)	TiO_2 (4)	56 (56.5)	3SiC–4TiC (72.7)
1b (3)	TiO_2 (4)	60 (59.2)	6SiC–4TiC (57.1)
1c (1)	TiO_2(4)	51 (49.1)	SiC–4TiC (88.9)
1a (3)	ZrO_2 (4)	62 (65.5)	SiC–4ZrC[c] (77.4)
1a (3)	HfO_2 (4)	71 (76.0)	3SiC–4HfC[d] (86.4)
1a (13)	V_2O_5 (8)	52 (52.2)	13SiC–$4V_4C_3$ (64.8)
1a (7)	Nb_2O_5 (4)	62 (62.1)	7SiC–8NbC (74.9)
1a (7)	Ta_2O_5 (4)	72 (72.6)	7SiC–8TaC (84.6)
1a (7)	MoO_3 (8)	59 (58.7)	7SiC–4Mo_2C (74.4)
1a (1)	WO_3 (1)	69 (69.8)	SiC–WC (83.0)

[a]Theoretical values in parentheses. [b]Determined both by IR spectroscopy and XRD. [c]For a total conversion of ZrO_2 into ZrC, pyrolysis times were increased up to 5 h. [d]For a total conversion of HfO_2 into HfC, pyrolysis times were increased up to 7 h.

Table 8 SiC/metal silicide pyrolysis products (type **B**, under argon)

Polymer **1a** (equiv.)	Metal oxide (equiv.)	Ceramic yield (%)	Phases characterized by XRD
(3)	Co_3O_4 (1)	54	CoSi
(1)	NiO (2)	61	Ni_2Si
(1)	PdO (4)	78	Pd_3Si–Pd_4Si
(1)	PtO_2 (2)	64	Pt_3Si–Pt_5Si

purges, the samples were pyrolyzed in a tube furnace under a continuous flow of argon or nitrogen at a flow rate of 90 mL min^{-1}. The temperature was increased at a heating rate of 5 °C min^{-1} from room temperature to 250 °C and then at 10 °C min^{-1} to 1400 °C. The final temperature was held for a variable period (2–7 h), and then cooled to room temperature. The pyrolysis conditions and compositions of the resulting powders are summarized in Tables 7–10.

2.4.1. Elemental analyses of the ceramics obtained from pyrolysis under an inert atmosphere (argon). *2.4.1.1. SiC/metal carbide ceramics (from dipersions of type **A**).* SiC/TiC; found: $Ti_{4.00}Si_{2.98}C_{6.51}O_{0.15}$; calcd: $Ti_{4.00}Si_{3.00}C_{7.00}$. SiC/ZrC; found: $Zr_{4.00}Si_{2.85}C_{7.14}O_{0.37}$; calcd: $Zr_{4.00}Si_{3.00}C_{7.00}$. SiC/NbC; found: $Nb_{8.00}Si_{4.82}C_{17.60}O_{0.52}$; calcd: $Nb_{8.00}Si_{7.00}C_{15.00}$. SiC/$Mo_2C$; found: $Mo_{8.00}Si_{6.84}C_{15.93}O_{0.24}$; calcd: $Mo_{8.00}Si_{7.00}C_{15.00}$. SiC/HfC; found: $Hf_{4.00}Si_{2.63}C_{6.23}O_{0.45}$; calcd: $Hf_{4.00}Si_{3.00}C_{7.00}$. SiC/WC; found: $W_{1.00}Si_{0.92}C_{2.14}O_{0.02}$; calcd: $W_{1.00}Si_{1.00}C_{2.00}$.

*2.4.1.2. Metal silicide ceramics (from dispersions of type **B**).* CoSi/C; found: $Co_{1.00}Si_{1.08}C_{2.91}O_{0.06}$; calcd: $Co_{1.00}Si_{1.00}C_{3.00}$. Ni_2Si/C; found: $Ni_{2.00}Si_{1.18}C_{2.71}O_{0.12}$; calcd: $Ni_{2.00}Si_{1.00}C_{3.00}$. Pd_3Si/Pd_4Si/C; found: $Pd_{1.00}Si_{0.26}C_{0.85}O_{0.03}$; calcd: $Pd_{1.00}Si_{0.25}C_{1.00}$.

2.4.2. Elemental analyses of the ceramics obtained from pyrolysis under a reactive atmosphere (N_2). SiC/AlN; found: $Al_{8.00}Si_{2.94}C_{3.89}N_{6.75}O_{0.96}$; calcd: $Al_{8.00}Si_{3.00}C_{3.00}N_{8.00}$. SiC/$Si_3N_4$; found: $Si_{9.00}C_{2.92}N_{8.13}O_{0.32}$; calcd: $Si_{9.00}C_{3.00}N_{8.00}$. SiC/TiN; found: $Ti_{2.00}Si_{1.04}C_{1.46}N_{2.04}O_{0.21}$; calcd: $Ti_{2.00}Si_{1.00}C_{1.00}N_{2.00}$. SiC/HfN; found: $Hf_{2.00}Si_{0.62}C_{1.16}N_{1.98}O_{0.48}$; calcd: $Hf_{2.00}Si_{1.00}C_{1.00}N_{2.00}$.

2.4.3. Elemental analyses of the ceramics obtained from pyrolysis under a reactive atmosphere (ammonia). Si_3N_4/TiN; found: $Ti_{6.00}Si_{2.24}N_{8.06}O_{1.18}$; calcd: $Ti_{6.00}Si_{3.00}N_{9.00}$. Si_3N_4/ZrO_2; found $Zr_{6.00}Si_{2.02}N_{3.58}O_{11.03}$; calcd: $Zr_{6.00}Si_{3.00}N_{4.00}$. Si_3N_4/HfO_2; found $Hf_{6.00}Si_{2.06}N_{3.03}O_{11.96}$; calcd: $Hf_{6.00}Si_{3.00}N_{4.00}$.

3. Results and discussion

3.1 Poly[(silylene)diacetylenes] as SiC/C ceramic sources: structural investigations

Fig. 1 shows the XRD patterns of ceramics derived from polymers **1a** and **1c** pyrolyzed at 1400 °C for 1 h under argon. In each case, the three broad peaks which are observed at $2\theta = 36°$, 60° and 72° correspond to the (111), (220) and (311) planes of β-SiC respectively. The very broad peak which is well observed for SiC–12C at $2\theta = 22°$ is attributed to amorphous graphitic carbon. The peak widths were used to calculate the average β-SiC particle sizes which are given with the free carbon content in Table 11. In spite of high temperature treatments, it may be pointed out that β-SiC is present as nanocrystals in the final residue. This result is related to the large amounts of free carbon present along with SiC, which acts as a crystal-growth inhibitor during the thermal precursor-to-ceramic conversion.[15,42]

Since bulk silicon carbide is known to be oxygen-resistant at high temperature,[43,44] we have investigated the thermal air-oxidation behavior of the residue obtained from the pyrolysis of **1a** at 1400 °C under argon (SiC–4C). Surprisingly, if a sample of the SiC–4C ceramic is exposed to flowing air at 1400 °C a white residue identified as pure SiO_2 is recovered. TGA curve in the 20–1400 °C temperature range (Fig. 2) showed the succession of two steps. The initial weight loss (50%) which occurred in the 450–750 °C domain was assigned to the air oxidation of the free carbon (theoretical value for 4C: 54.5%). Above 750 °C, the weight increase (20%) was indicative of the air-oxidation of SiC into SiO_2 as determined by XRD. The overall weight loss of 30.3% is close to the expected value (31.8%) for the conversion SiC–4C→SiO_2. When compared to the pure bulk material, the total oxidation of the silicon carbide at such a low temperature is consistent with

Table 9 SiC/metal nitride pyrolysis products (under nitrogen)

Polymer **1a** (equiv.)	Metal oxide (equiv.)	Ceramic yield[a] (%)	Stoichiometry of the ceramic[b] (MN [%])
(1)	TiO_2 (2)	64 (62)	SiC–2TiN (75.6)
(1)	ZrO_2 (2)	66 (71)	SiC–2ZrN (84.0)
(1)	HfO_2 (2)	84 (81)	SiC–2HfN (90.6)
(5)	V_2O_5 (4)	58 (57)	5SiC–8VN (72.2)
(5)	Nb_2O_5 (4)	71 (66)	5SiC–2$Nb_4N_{3.92}$ (81.0)
(3)	Al_2O_3 (4)	62 (62)	3SiC–8AlN (73.2)
(1)	SiO_2 (2)	62 (59)	SiC–2/3Si_3N_4 (70.0)

[a]Theoretical values in parentheses. [b]Determined both by IR spectroscopy and XRD.

Table 10 Si_3N_4-based pyrolysis products (under ammonia)

Polymer **1a** (equiv.)	Metal oxide (equiv.)	Ceramic yield[a] (%)	Composition of the ceramic[b]
(1)	TiO_2 (2)	59 (64)	Si_3N_4–TiN
(1)	ZrO_2 (2)	78 (83)	Si_3N_4–ZrO_2
(1)	HfO_2 (2)	84 (89)	Si_3N_4–HfO_2
(5)	Nb_2O_5 (4)	65 (68)	Si_3N_4–NbN–$Nb_4N_{3.92}$
(5)	Ta_2O_5 (4)	80 (78)	Si_3N_4–TaN–TaON
(3)	Al_2O_3 (4)	70 (75)	Si_3N_4–Al_2O_3–AlON

[a]Theoretical values in parentheses. [b]Determined both by IR spectroscopy and XRD, phases are given in order of abundance.

Table 11 Calculated β-SiC particle sizes after pyrolysis at 1400 °C under argon

Polymer	Ceramic stoichiometry	Calculated β-SiC particle size/nm	Free C content (%)
1a	SiC–4C	3.4	54.5
1c	SiC–12C	2.2	78.3

the nanometer size of the crystallites present in the material. Therefore, we suggest that the silicon oxide coating film responsible for the oxidation resistance has the same extent as the particle itself.

For a complete characterization of the microstructure of these ceramic samples, we turned to scanning (SEM) and transmission (TEM) electron microcopies. SEM micrographs of the ceramics resulting from the pyrolysis of **1a** (SiC–4C) and **1c** (SiC–12C) at 1400 °C under argon are shown in Fig. 3. The surface of the SiC–4C ceramic (Fig. 3a) appeared to be chaotic and highly porous. In contrast to this observation, the SiC–12C ceramic was shown to be quite different. The smooth surface of the sample was drilled by round-shaped pores indicative of the evolution of gases in a semi-molten state during the pyrolysis. Consistent with these observations, the surface areas obtained from BET analyses were 407 $m^2\ g^{-1}$ for SiC–4C and 18 $m^2\ g^{-1}$ for SiC–12C.

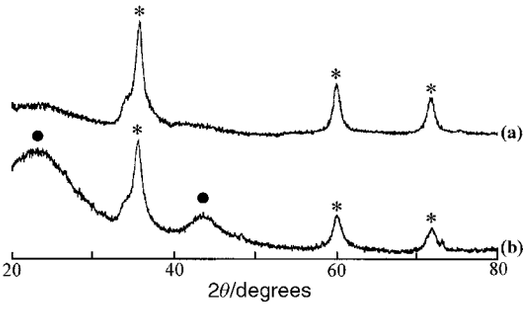

Fig. 1 XRD patterns of the ceramics resulting from the pyrolysis under argon at 1400 °C of (a) polymer **1a** and (b) polymer **1c** (*: β-SiC; ●: C).

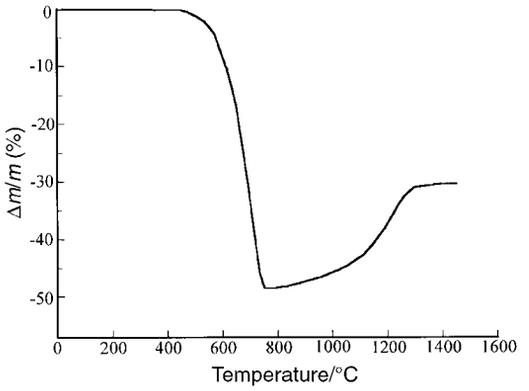

Fig. 2 TGA curve of SiC–4C pyrolyzed under air to 1400 °C.

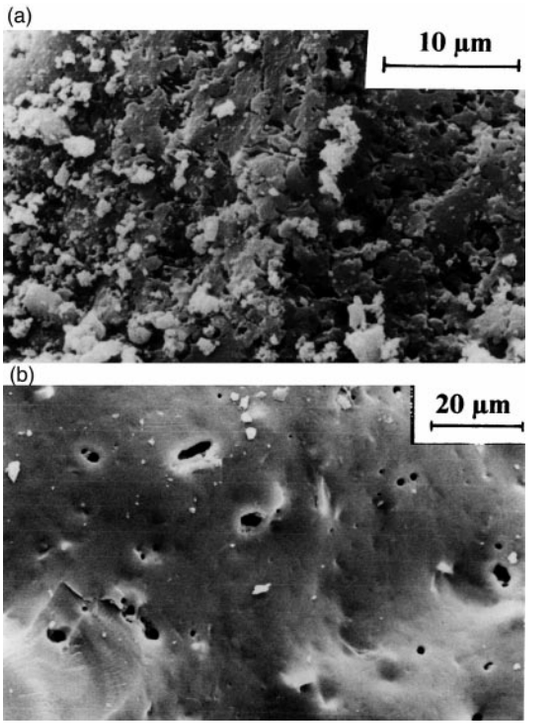

Fig. 3 SEM micrographs of (a) SiC–4C and (b) SiC–12C ceramics pyrolyzed at 1400 °C under argon.

The high magnification TEM bright-field micrograph of a sample of **1a** heated at 800 °C (Fig. 4a) showed a very homogeneous microstructure throughout all the grains. At 1400 °C, the images showed a quite different microstructure (Fig. 4b). Small dark aggregates (size <5 nm) were regularly dispersed throughout an amorphous matrix. From both dark-field images and selected area electron diffraction (SAED) the aggregates were identified to be crystalline β-SiC. The TEM micrograph of the SiC–12C ceramic (Fig. 4c) showed a similar microstructure constituted of nanocrystals of β-SiC (*ca.* 2 nm) embedded in an amorphous carbon matrix.

3.2. Metal oxide/polymer dispersions: preparation and characterization

Taking advantage of the above properties, we decided to use poly[(silylene)diacetylenes] as wrapping and reactive polymers towards metal oxide particles. Our approach is the following: i) polymers **1** are soluble in common organic solvents: thus the encapsulation of the metal oxide particles by the polymer may be easily achieved, ii) the solid-state thermosetting crosslinking reaction of polymers **1** at about 200 °C would prevent the sedimentation of the wrapped metal oxide particles, and iii) the thermal conversion of the preceramic polymer acting as an *in situ* carbon source/metal oxide dispersion should result in both the carbothermal reduction of encapsulated oxide particles and the formation of SiC to afford mixed carbides as ceramic residues.

The metal oxide/polymer dispersions were prepared by adding the appropriate metal oxide to a THF solution of the polymer, followed by vacuum evaporation of the solvent under vigorous stirring. A typical TEM image of **1a**/TiO_2 dispersions (Fig. 5a) exhibited evidence of submicron TiO_2 particles embedded in a matrix composed of **1a**.

3.3. Pyrolysis under an inert atmosphere (argon)

3.3.1. Pyrolysis of dipersions of type A (see Table 3): synthesis of SiC/metal carbide ceramics. The preceramic polymer approach is quite general and a wide range of materials can

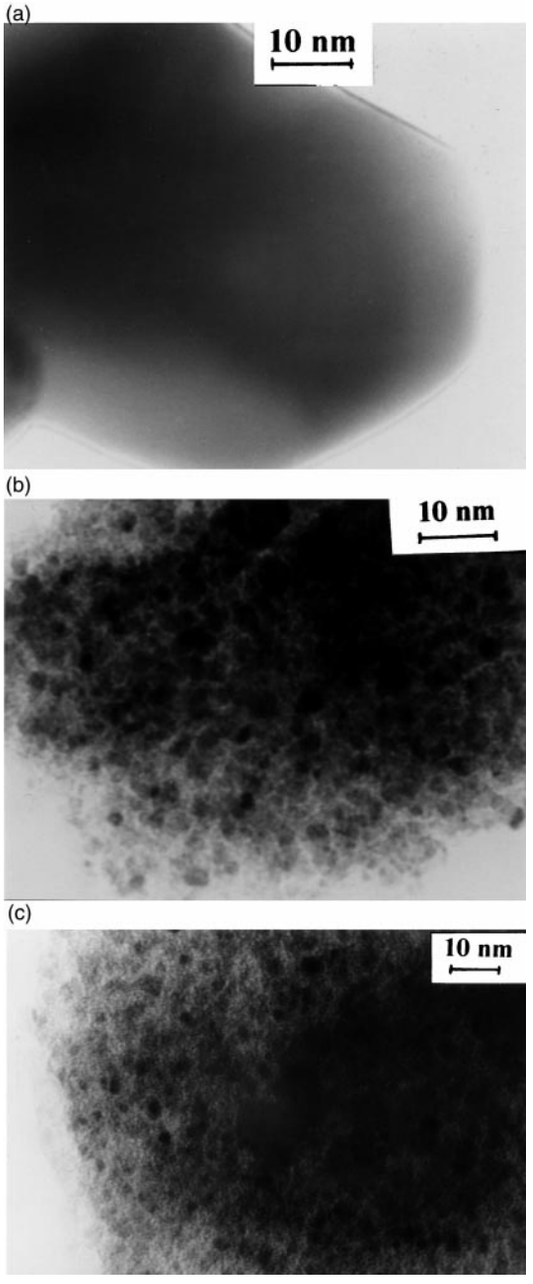

Fig. 4 TEM micrographs of (a) **1a** pyrolyzed at 800 °C, (b) **1a** pyrolyzed at 1400 °C and (c) **1c** pyrolyzed at 1400 °C under argon.

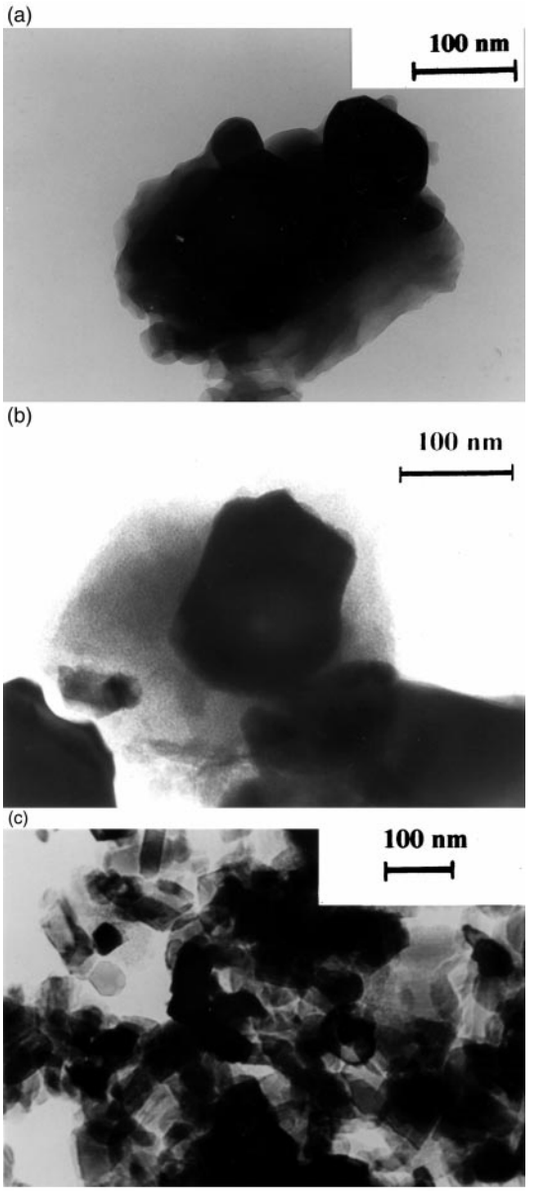

Fig. 5 TEM micrographs of a **1a**/TiO_2 dispersion at (a) room temperature, (b) 1000 °C and (c) 1400 °C for 2 h.

be easily obtained (Table 7). Under similar experimental conditions, the pyrolysis of various **1a**/metal oxide dispersions in an argon flow gave high yields of crystalline phases that contained the respective metal carbide and SiC in a well defined ratio. As an example, Fig. 6 shows the XRD pattern of the ceramic resulting from the pyrolysis of a **1a**/Nb_2O_5 dispersion at 1400 °C for 2 h in which SiC and NbC are present as the unique phases of the ceramic. The cell parameters of the metal carbides which were calculated from the indexing of the diffraction peaks clearly indicated the total conversion of the initial metal oxide into the final carbide. The IR spectra (Fig. 7) revealed only the characteristic absorption of SiC at about 820 cm^{-1}. No absorption that could be assigned to unreacted oxide-based amorphous phases could be found in the 450–1100 cm^{-1} region.[45,46] Moreover, the following points have to be highlighted: i) the reaction of the SiC–4C matrix with the metal oxide takes place at lower temperatures than with carbon alone whatever the nature of the oxide; for instance, in the case of the refractory ZrO_2 and HfO_2, the reported processing temperatures range between 2000 and 2500 °C,[1,47] ii) the carbothermal reduction kinetics appeared to be faster than for conventional powder processes.[1,47]

A TEM micrograph for SiC/TiC (Fig. 5c) showed that the material is mainly formed of submicron crystallites. Analyses

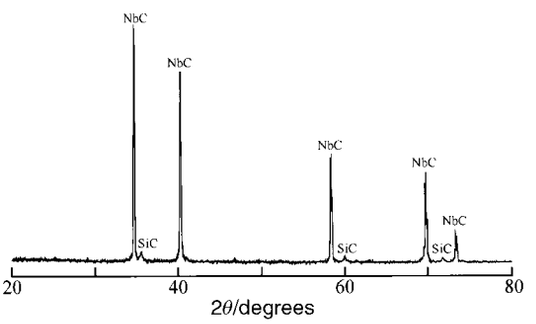

Fig. 6 X-Ray diffraction pattern of a SiC/NbC ceramic resulting from the pyrolysis of a **1a**/Nb_2O_5 dispersion at 1400 °C for 2 h under argon.

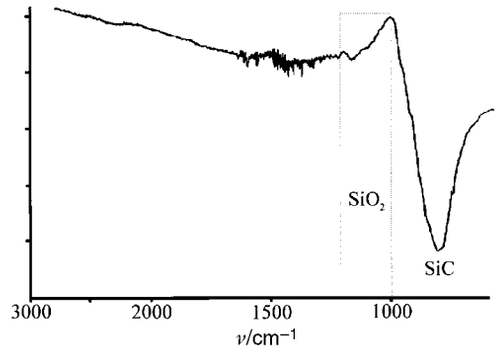

Fig. 7 Typical IR spectrum (KBr pellets) of SiC/MC ceramics heated at 1400 °C for 2 h under argon.

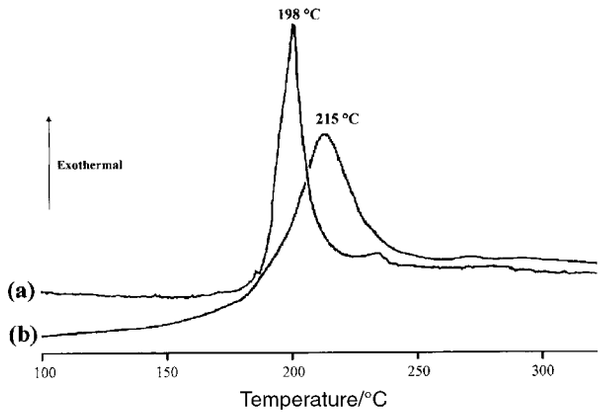

Fig. 8 DSC curves of (a) polymer **1a** alone and (b) a **1a**/TiO_2 composite.

by means of dark-field imaging associated with SAED gave no evidence for residual material (free carbon, titanium oxides) to be present; the spots corresponding to the TiC lattice are only observed. This is most likely due to either similarity in the cell parameter between β-SiC and TiC or a poor crystallinity, the electron diffraction patterns associated with β-SiC are not observed by this method. Nevertheless, the EDX analysis conducted on several isolated particles exhibited the Ti/Si ratio (3/4) initially present in the starting precursor. Similar results have been obtained with the other ceramics. The slight grain size and morphology differences which are observed likely originated from the particle size and morphology of the starting metal oxide. The nitrogen adsorption–desorption isotherms obtained with this sample are typical of a microporous substance.[48] Thus, the value of the specific area of 273 $m^2\ g^{-1}$, which was appreciably greater than those reported for conventional ceramics,[49] may originate from both the particle size and the presence of surface porosity. BET measurements conducted on the other SiC/MC ceramics always showed specific areas greater than 120 $m^2\ g^{-1}$.

The micrograph (Fig. 5b) revealed that the reactive matrix containing SiC intimately encapsulates the oxide particles at 1000 °C. Thus, according to the above results, one can conclude that after the completion of the carbothermal reduction, the SiC phase is present as a porous crust at the surface of the metal carbide particles. Moreover, this assumption is reasonable since β-SiC, which adopts a diamond-like cubic structure, cannot form solid solutions with metal carbides of this series which are known to have a rock salt-like cubic structure.

As described previously for a **1a**/TiO_2 dispersion,[23] two main weight losses were observed during the pyrolysis of all the studied samples. The initial weight loss, consistent with the polymer decomposition [eqn. (1)] occurred in the 450–750 °C range and was accompanied by the evolution of methane and hydrogen as detected by mass spectroscopy.

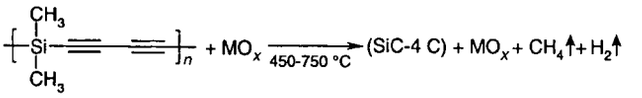

(1)

The second weight loss took place at temperatures higher than 1200 °C, and was attributed to the carbothermal reduction of the starting oxide into the final metal carbide [eqn. (2)]. In this temperature domain, only CO was detected by mass spectroscopy. Finally, in each case, the overall weight loss is close to the value calculated for the transformation: a**1a** + $bMO_x \rightarrow aSiC + bMC_y$ and consistent with a complete carbothermal reduction of the metal oxide.

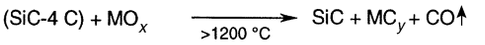

(2)

As exemplified with a **1a**/TiO_2 precursor, DSC analyses up to 350 °C only revealed the presence of an additional phenomenon characterized by a strong exotherm at 215 °C (Fig. 8). As mentioned above, this transformation is related to the polymer cross-linking through the diacetylenic units leading to the irreversible encapsulation of the oxide particles. When compared to the DSC curve obtained for the polymer **1a** alone, the curve obtained for the precursor dispersions shows, first a significant broadening of the exothermic peak and second, a slight displacement of the maximum to higher temperatures (Fig. 8). As described previously,[36] these observations may arise from the combination of two effects, first a lack of crystallinity in the polymer which would disfavor the polyaddition of the diacetylenic units, and second a dilution afforded by the presence of the metal oxide particles. On the other hand, the peak integration shows that the presence of the TiO_2 particles did not affect significantly the exothermicity of

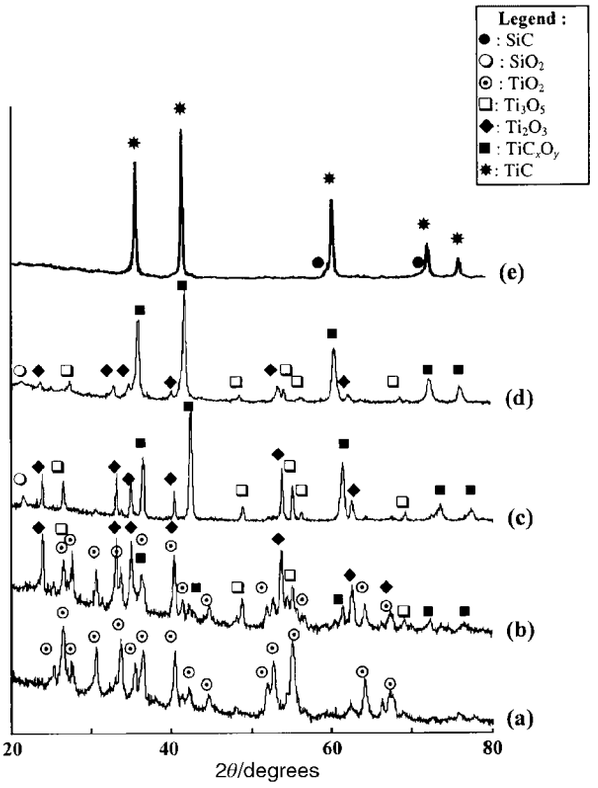

Fig. 9 X-Ray diffraction patterns of a **1a**/TiO_2 dispersion heated under argon at (a) 1000 °C for 10 min, (b) 1200 °C for 10 min, (c) 1300 °C for 10 min, (d) 1400 °C for 10 min, (e) 1400 °C for 2 h.

the crosslinking reaction, *i.e.*, 80 kJ mol^{-1} for **1a** *versus* 82 kJ mol^{-1} for **1a** in the dispersion.

In the 1000–1400 °C temperature range, the ceramic conversion processes were followed by X-ray diffraction techniques. The patterns of the ceramics prepared starting from **1a**/TiO_2 at different temperatures are shown in Fig. 9. When the precursor was heated at 1000 °C for 10 min (Fig. 9a), the material was found to be mainly composed of anatase and rutile allotropes of TiO_2. On increasing the temperature, new crystallized phases appeared. At 1200 °C (Fig. 9b) beside TiO_2, the presence of the suboxide phases Ti_3O_5, Ti_2O_3 and TiC_xO_y[50] indicated that the carbothermal reduction process had taken place. At 1300 °C (Fig. 9c), a total disappearance of TiO_2 was noticed. The presence of α-SiO_2 may be related to the reaction between the nascent SiC resulting from the degradation of **1a** and titanium oxides, which resulted in the formation of titanium oxycarbide [eqn. (3)]. This result is consistent with the relative reactivity of the so-formed SiC toward oxygen as outlined above. Finally, the titanium carbide, which is unambiguously observed at 1400 °C, reached its optimal cell parameter after 2 h at this temperature (Fig. 9e).

$$SiC + 2\ TiO_2 \longrightarrow SiO_2 + 2\ TiOC \quad (3)$$

The above observations can be extended to the other samples: except for ZrO_2 and HfO_2, the carbothermal reduction of the other metal oxides occurred through a series of intermediate suboxides.

Finally, changing the nature of the substituents at the silicon atoms allowed the modification over a large range of the SiC/MC ratio, since the excess of carbon content depends on R_2Si (Table 1). As shown in Table 7, when aryl groups are bonded to silicon (polymer **1c**), ceramics containing higher amounts of TiC result (88.9%). In contrast, a **1b**/TiO_2 dispersion produced a ceramic with a lower TiC content (57%).

3.3.2. Pyrolysis of dispersions of type B (see Table 4): synthesis of metal silicides/C ceramics. Following the same procedure, the materials resulting from the pyrolysis of precursors of type **B** display noticeable differences. First of all, since they are not thermodynamically stable as metal carbides, only the corresponding metal silicides and graphitic carbon were detected by XRD (Table 8). Moreover, the absence of either silicon oxides or silicon carbide was confirmed by infrared spectroscopy. Second, as exemplified with a $PtSi_x$/C ceramic, the MEB micrographs (Fig. 10) showed a quite heterogeneous structure at the micron scale. EDX analyses showed that the spherical clear particles were constituted of Pt and Si in a ratio close to the initial composition of the precursor (2 : 1), whereas the dark matrix was formed of pure carbon. Further investigations of the latter phase using TEM clearly showed that it mainly displayed a turbostratic graphitic structure.

The thermal transformations of these dispersions can be summarized as follows: the two first steps of the pyrolysis, namely the reticulation of the initial polymer and the subsequent mineralization of the organometallic matrix, occurred in the same temperature domains as observed for the precursors of type **A**. At higher temperatures, the onset of the carbothermal reduction depended on the nature of the metal and led to the observation of free metal by XRD [eqn. (4)]. On further heating, as described previously,[51,52] the metal silicides were formed through the reaction of SiC with the metal particles with the release of graphitic carbon [eqn. (5)].[53,54]

$$a\ \mathbf{1a} + b\ MO_x \xrightarrow[<1000\ °C]{} a\ SiC + b\ M + c\ C + \ldots \quad (4)$$

$$SiC + M \xrightarrow[>1000\ °C]{} MSi_x + C_{(graphite)} \quad (5)$$

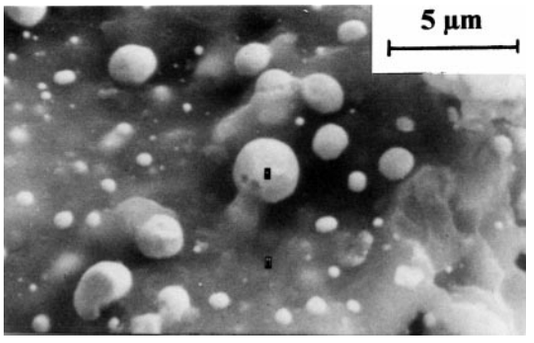

Fig. 10 SEM micrograph of Pt/Si/C ceramic resulting from the pyrolysis of a **1a**/PtO_2 dispersion pyrolyzed at 1400 °C under argon.

3.4. Pyrolysis under reactive atmospheres

3.4.1. Pyrolysis under nitrogen: synthesis of SiC/metal nitride ceramics. It is well known that the carbothermal reduction of some metal oxides under N_2 gives nitrides.[1] This reaction occurs at temperatures above 1100 °C as illustrated for TiO_2 in eqn. (6).[55–57]

$$TiO_2 + 2\ C + 1/2\ N_2 \xrightarrow[T>1100\ °C]{} TiN + 2\ CO\uparrow \quad (6)$$

We may expect to prepare SiC–metal carbide mixed ceramics; each component will be obtained from different pathways. Whatever the atmosphere (Ar, N_2),[47] SiC is formed from the preceramic polymer through a re-organization of the bonds around the silicon atoms. On the other hand, the nitride phase will result from the carbothermal reduction of the metal oxide and its nitridation by nitrogen.

The experimental procedure was the same as described previously except that the flow of argon is replaced by a flow of nitrogen. A wide range of ceramics of defined compositions were obtained (Table 9). The observations made during the pyrolysis under argon can be transposed when using these new experimental conditions and are summarized as follows: i) the materials were obtained with high ceramic yields quite close to the expected values, ii) the reactions occurred at lower

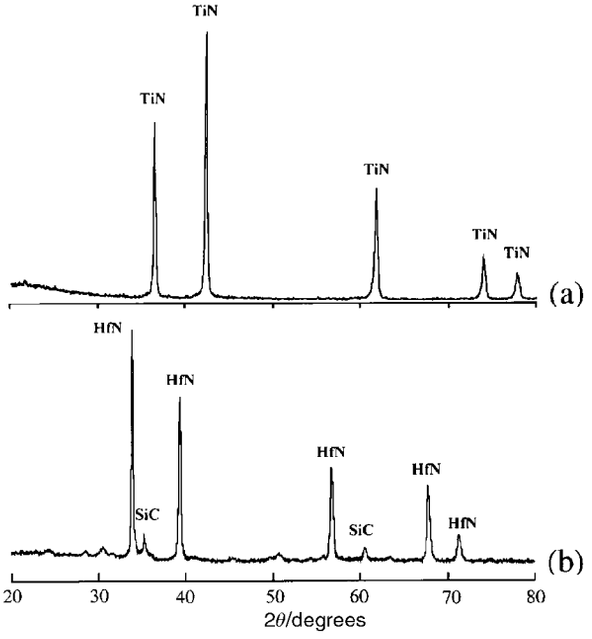

Fig. 11 XRD pattern of (a) a **1a**/TiO_2 dispersion pyrolyzed under nitrogen at 1400 °C for 0.5 h and (b) a **1a**/HfO_2 dispersion pyrolyzed under nitrogen at 1500 °C for 5 h.

temperatures and with an improved kinetic, iii) the variations in the starting polymer allow the modulation of the metal nitride content in the final material.

As examples, Fig. 11 shows the XRD patterns of the materials obtained from the pyrolysis under N_2 of a **1a**/TiO_2 dispersion at 1400 °C for 2 h and of a **1a**/HfO_2 dispersion at 1500 °C for 5 h. From the indexing of the peaks, the corresponding metal nitrides were unambiguously identified. Moreover the observed value of the nitrides cell parameter indicated that the carbothermal reduction and nitridation of the metal oxide into the metal nitride were achieved quantitatively; carbonitride-type solid solutions were not obtained. In contrast to the β-SiC/TiN ceramic for which the cell parameters of SiC and TiN are quite close, the diffraction peaks associated to β-SiC were observed for the SiC/HfN material. Nevertheless the absorption characteristic of β-SiC at 820 cm^{-1} was clearly observed in the IR spectrum in all cases.

As shown by thermal analysis, the pyrolysis pathways of a **1a**/metal oxide dispersions were similar under argon or under nitrogen [eqn. (7)]. The first weight loss between 450 and 800 °C was consistent with the conversion of the dispersion into a SiC–4C/metal oxide composite; above 1200 °C, the second weight loss was associated to the carbothermal reduction–nitridation processes leading to the final SiC/metal nitride material.

$$\mathbf{1a} + 2\,TiO_2 + N_2 \xrightarrow[>1200\ °C]{} SiC + 2\,TiN + CH_4\uparrow + H_2\uparrow + 4\,CO\uparrow \quad (7)$$

The XRD studies conducted on samples pyrolyzed in the 1000–1400 °C domain showed a sequence of crystallized intermediate phases similar to those which have been already reported for mixtures of powders.[55–57] At 1000 °C, the allotropic transformation of TiO_2 (anatase) into TiO_2 (rutile) took place and was followed at 1200 °C by an increase of the relative amount of Ti_3O_5 with respect to TiO_2. The latter completely disappeared at 1300 °C, and titanium oxynitride was formed. The presence of titanium oxynitride was only observed near 1400 °C and finally TiN achieved its optimal cell parameter (4.24 Å) at 1400 °C for 0.5 h.

3.4.2. Pyrolysis under ammonia: synthesis of Si_3N_4 based ceramics. Finally, the potential of the preceramic polymer route was investigated using a reactive atmosphere of ammonia. As described previously,[35] the pyrolysis of **1a** at 1400 °C under an ammonia flow is known to afford silicon nitride as a residue. The organometallic–inorganic transformation involved first, both the thermal decomposition of the cross-linked material and the reaction with ammonia leading to the formation of the Si_3N_4 network inside a material of a composition close to $SiNC_4$ (400–700 °C), and second, the consumption of the carbon matrix with the evolution of HCN (>750 °C) leading to crystallized Si_3N_4 at 1400 °C. Thus, two approaches may be reasonably envisioned. In the first one [eqns. (8)–(10)], we shall take advantage of the excess of carbon which is present beside Si_3N_4 at 700 °C. Changing ammonia to argon or nitrogen at this temperature in order to avoid the carbon consumption (*vide supra*) should allow the carbothermal reduction of the entrapped oxide particles; on further heating, Si_3N_4/metal carbide or nitride ceramics would be finally obtained. A second approach [eqn. (11)] will take advantage of the ability of some finely dispersed metal oxide powders to form metal nitride when heated under an ammonia atmosphere.[58,59] Thus, the pyrolysis of such **1a**/metal oxide dispersion would afford Si_3N_4/metal nitride ceramics.

$$a\,\mathbf{1a} + b\,MO_x \xrightarrow[<700\ °C]{NH_3} a\,SiNC_4 + b\,MO_x + CH_4\uparrow + H_2\uparrow \quad (8)$$

$$a\,SiNC_4 + b\,MO_x \xrightarrow[700\text{-}1400\ °C]{Ar} a/3\,Si_3N_4 + b\,MC_y + x\,CO\uparrow \quad (9)$$

$$a\,SiNC_4 + b\,MO_x \xrightarrow[700\text{-}1400\ °C]{N_2} a/3\,Si_3N_4 + b\,MN_y + x\,CO\uparrow \quad (10)$$

$$a\,SiNC_4 + b\,MO_x \xrightarrow[700\text{-}1400\ °C]{NH_3} a/3\,Si_3N_4 + b\,MN_y + HCN\uparrow + H_2O\uparrow \quad (11)$$

In a typical experiment, we first carried out the pyrolysis of a **1a**/TiO_2 dispersion (ratio: 3 : 4) under ammonia up to 700 °C and then under argon up to 1400 °C for 2 h. The X-ray pattern showed that the dark-golden residue obtained under these conditions was composed of TiN instead of the expected TiC. Beside TiN, SiC was clearly identified by IR spectroscopy. Thus, the pyrolysis of the TiO_2 particles under argon by a molecular precursor to Si_3N_4/C composites allowed both the reduction of the oxide and its nitridation; the most thermodynamically stable phases SiC and TiN are only formed.

Using a continuous flow of ammonia, the pyrolysis of a **1a**/TiO_2 dispersion (ratio: 1 : 2) up to 1400 °C for 5 h, afforded a golden ceramic in 59% yield (theoretical yield: 64.2%). The analysis of the XRD pattern (Fig. 12) showed the presence of α-Si_3N_4 and TiN as the crystallized phases. In contrast to the pyrolysis performed either under argon or under nitrogen for which the metal/Si ratio remained constant, the elemental analysis of the residue showed 25% of silicon lost. If we consider the relatively high oxygen content of the ceramic (4%), we may invoke that a part of the silicon evolved as volatile silicon monoxide that could be due to a high-temperature oxidation related to the presence of either oxygen or moisture in the ammonia used here.[35]

The TG analyses (Fig. 13) showed a succession of three weight losses. The first one (400–750 °C) was consistent with both the nitrogen incorporation and the mineralization of the matrix leading to a material of composition $SiC_4N/2TiO_2$ (weight losses: experimental: 6%, theoretical: 5.9%). The second loss (750–1000 °C) was attributed to the consumption of the excess carbon with the evolution of HCN leading to the formation of a silicon nitride/TiO_2 composite (weight losses: experimental: 20%, theoretical: 17.2%). Finally both the carbothermal reduction and nitridation of TiO_2 into TiN took place above 1100 °C and gave the expected α-Si_3N_4/TiN ceramic (weight losses: experimental: 16%, theoretical: 17.2%).

The pyrolysis results of some **1a**/metal oxide precursors under similar experimental conditions are given in Table 10. The examination of the ceramic compositions, as determined

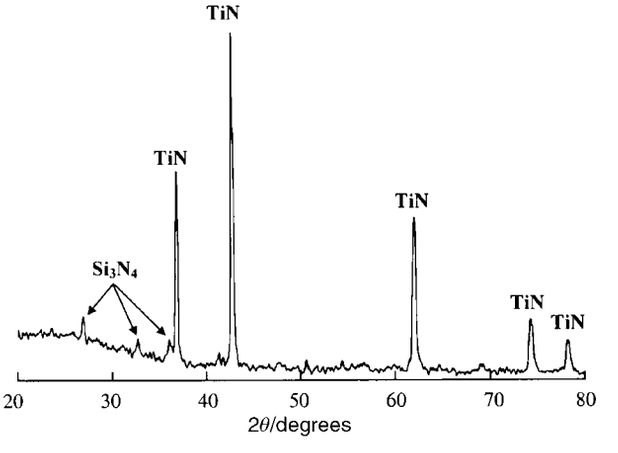

Fig. 12 XRD pattern of a **1a**/TiO_2 dispersion pyrolyzed at 1400 °C for 5 h under ammonia.

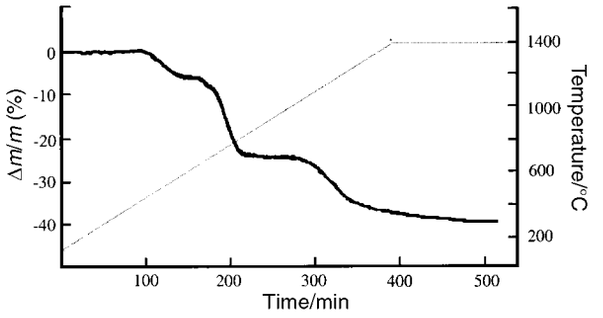

Fig. 13 TG curve obtained during the pyrolysis of a **1a**/TiO_2 composite under ammonia.

from their XRD patterns, allowed the definition of two classes of precursors. In the first one (TiO_2, Nb_2O_5, Ta_2O_5), beside Si_3N_4 which was observed in every case, the reduction–nitridation of the starting metal oxide by the thermal decomposition products of NH_3 appeared to be quite efficient. In the case of the **1a**/Ta_2O_5 precursor, the oxynitride TaON which is detected in small amounts (<5%), probably resulted from an incomplete reduction due to an insufficient pyrolysis duration. In the second class (Al_2O_3, ZrO_2, HfO_2), the reduction–nitridation of the starting metal oxide was either ineffective or weak as in the case of Al_2O_3 where 5–10% of crystallized aluminium oxynitride were detected.

3.5. Effect of the carbon matrix on the carbothermal reduction

As outlined above, the carbothermal reduction of the oxide particles wrapped by the reactive SiC–*n*C matrices always occurred at lower temperature and with an improved kinetic when compared to the data reported for mixtures of powders.[1,47] In order to appreciate more precisely the improvements afforded by the particle encapsulation itself, we have performed the pyrolysis under argon of an intimate SiC–4C/TiO_2 mixture (ratio 3:4).[61] Fig. 14 shows the high-temperature-domain ($T>1000\,^{\circ}C$) TGA curves for TiO_2 encapsulated by SiC–4C and TiO_2 mixed with SiC–4C. It is obvious that at 1500 °C, the carbothermal reduction of the oxide particles wrapped inside the reactive matrix was complete (weight loss, observed: 38%, expected: 38.4%) whereas 30% in weight of unreacted oxide was observed at this temperature in the powder route. Moreover, the onset of the carbothermal process for the latter approach occurred 135 °C above the temperature required in the metal oxide/polymer system. This clearly indicates that the *in situ* generation of the reactants resulting from the pyrolysis of metal oxide particles wrapped by polymers **1** does lead to improved reaction conditions. As shown above, the encapsulation of the oxide particles remained stable even after the mineralization of the matrix into SiC/C leading to an intimate contact between the reactants. Consequently, the reaction temperature is substantially lowered.

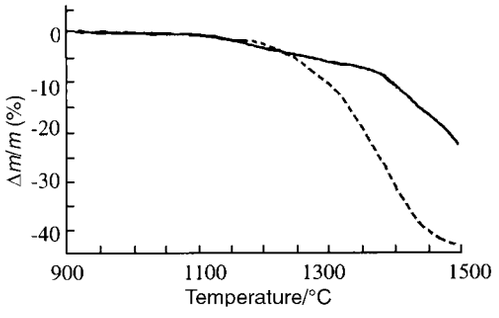

Fig. 14 TG curves obtained during the pyrolysis under argon of a **1a**/TiO_2 dispersion (dashed line) and of a SiC–4C/TiO_2 mixture (continuous line).

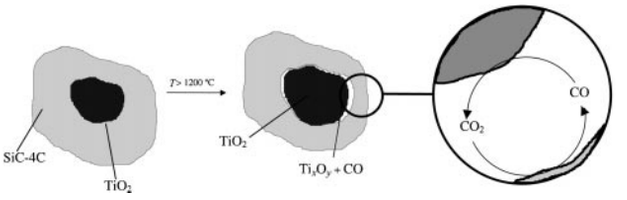

Fig. 15 Schematic representation of the particle-tailored micro-scale reactors.

Such improvements have been also found during the carbothermal synthesis of TiC using ultrafine TiO_2 particles coated by pyrolytic carbon.[48,62] It was pointed out that the key step lies in the initial solid-state surface reaction between TiO_2 and the carbon [eqn. (12)]. The evolved CO plays the double role of reducing agent and of a gas-phase carbon carrier through its reduction with the unreacted carbon [eqns. (13)–(14)].[47,61] Similarly as depicted in Fig. 15, the encapsulation of the oxide particles inside a reactive matrix led to the formation of particle-tailored micro-scale reactors in which the reduction process took place with high efficiency.

$$a\,TiO_2(s) + b\,C(s) \longrightarrow c\,Ti_xO_y(s) + d\,CO(g) \quad (12)$$

$$a\,TiO_2(s) + b\,CO(g) \longrightarrow c\,Ti_xO_y(s) + d\,CO_2(g) \quad (13)$$

$$CO_2(g) + C(s) \longrightarrow 2\,CO(g) \quad (14)$$

4. Conclusion

We have shown that the pyrolysis of preceramic polymer/metal oxide dispersions resulted in the formation of various silicon-based mixed ceramics of defined composition. First, by changing the pyrolysis atmosphere, SiC/metal carbides, metal silicides/C (under argon), SiC/metal nitrides (under nitrogen), Si_3N_4/metal nitrides or oxynitrides (under ammonia) have been prepared. Second, changing the preceramic polymer, it is possible to modulate the composition of the final ceramic. Moreover, we have shown that the materials described therein did not consist of particles of β-SiC beside particles of metal carbide (or nitride), but are constituted of particles containing both the discrete phases. These observations reflected the way of formation of these materials. We have afforded an argumentation for the encapsulation of the metal oxide particles inside the reactive polymeric matrix. The first pyrolysis step led to the formation of a highly cross-linked organometallic network which wrapped irreversibly the oxide particles. As a result, the overall carbothermal reduction occurred with a high efficiency inside micro-scale reactors containing an intimate mixture of silicon carbide, carbon and metal oxide. As a consequence, when compared to the data reported for the conventional powder technology, the composite ceramics described therein were obtained at lower temperatures and with improved kinetics.

Acknowledgements

The authors thank the CNRS for financial support. We are grateful to Dr Galy and Dr Baulès for TEM-EDX measurements and fruitful discussions.

References

1 L. E. Toth, *Transition Metal Carbides and Nitrides*, Academic Press, New York, 1971.
2 R. Riedel, E. Kroke, A. Greiner, A. O. Gabriel, L. Ruwisch and J. Nicolich, *Chem. Mater.*, 1998, **10**, 2964.

3 S. Dutremez, Ph. Gerbier, C. Guerin, B. Henner and Ph. Merle, *Adv. Mater.*, 1998, **10**, 465.
4 M. Itoh, K. Inoue, K. Iwata, J. Ishikawa and Y. Takenaka, *Adv. Mater.*, 1997, **9**, 1187.
5 R. Riedel and W. Dressler, *Ceram. Int.*, 1996, **22**, 233.
6 L. V. Interrante, Q. Liu and Q. Shen, *J. Organomet. Chem.*, 1996, **521**, 1.
7 E. Bacqué, M. Birot, J.-P. Pillot, P. Lapouyade, P. Gerval, C. Biran and J. Dunoguès, *J. Organomet. Chem.*, 1996, **521**, 99.
8 M. Birot, J.-P. Pillot and J. Dunoguès, *Chem. Rev.*, 1995, **95**, 1443.
9 J. Bill and F. Aldinger, *Adv. Mater.*, 1995, **7**, 775.
10 R. Riedel, *Naturwissenschaften*, 1995, **82**, 12.
11 R. J. P. Corriu, M. Enders, S. Huille and J. J. E. Moreau, *Chem. Mater.*, 1994, **6**, 15.
12 R. T. Paine, J. F. Janik and M. Fan, *Polyhedron*, 1994, **13**, 1225.
13 R. M. Laine and F. Baboneau, *Chem. Mater.*, 1993, **5**, 260.
14 D. R. Stanley, D. J. Birchall, J. N. K. Hyland, L. Thomas and K. Hodgetts, *J. Mater. Chem.*, 1992, **2**, 149.
15 W. R. Schmidt, L. V. Interrante, R. H. Doremus, T. K. Trout, P. S. Marchetti and G. E. Maciel, *Chem. Mater.*, 1991, **3**, 257.
16 B. Boury, L. Carpenter, R. J. P. Corriu and H. Mutin, *New J. Chem.*, 1990, **14**, 535.
17 N. S. Choong Kwet Yive, R. J. P. Corriu, D. Leclercq, H. Mutin, J.-M. Planeix and A. Vioux, *Organometallics*, 1990, **10**, 1457.
18 P. Greil, *J. Eur. Ceram. Soc.*, 1998, **18**, 1905.
19 D. Seyferth and P. Czubarow, *Chem. Mater.*, 1994, **6**, 10.
20 P. Greil, *J. Am. Ceram. Soc.*, 1995, **78**, 835.
21 R. J. P. Corriu, Ph. Gerbier, C. Guérin and B. Henner, *Adv. Mater.*, 1993, **5**, 380.
22 K. Su and L. G. Sneddon, *Chem. Mater.*, 1993, **5**, 1659.
23 R. J. P. Corriu, Ph. Gerbier, C. Guérin and B. Henner, *Angew. Chem., Int. Ed. Engl.*, 1992, **31**, 1195.
24 K. Su, M. Nowakowski, D. Bonnell and L. G. Sneddon, *Chem. Mater.*, 1992, **4**, 1139.
25 D. Seyferth, H. Lang, C. A. Sobon, J. Borm, H. J. Tracy and N. Bryson, *J. Inorg. Organomet. Polym.*, 1992, **2**, 59.
26 D. Seyferth, N. Bryson, D. P. Workman and C. A. Sobon, *J. Am. Ceram. Soc.*, 1991, **74**, 2687.
27 B. I. Lee and K. T. Chou, *Chemical Processing of Advanced Materials*, eds. L. L. Hench and J. K. West, J. Wiley & Son, Inc., New York, 1992, p. 753.
28 S. Yajima, T. Iwai, T. Yamamura, K. Okamura and Y. Hasegawa, *J. Mater. Sci.*, 1981, **16**, 1349.
29 J. F. Li and R. Watanabe, *J. Mater. Sci.*, 1991, **26**, 4813.
30 K. Thorne, E. Liimatta and J. D. Mackenzie, *J. Mater. Res.*, 1991, **6**, 2199.
31 A. Jalowiecki, J. Bill, M. Friess, J. Mayer, F. Aldinger and R. Riedel, *Nanostruct. Mater.*, 1995, **6**, 279.
32 K. W. Chae, K. Niihara and D.-Y. Kim, *J. Mater. Sci. Lett.*, 1995, **14**, 1332.
33 A. Dressler, A. Greiner, M. Seher and R. Riedel, *Nanostruct. Mater.*, 1995, **6**, 481.
34 R. J. P. Corriu, C. Guérin, B. Henner, A. Jean and H. Mutin, *J. Organomet. Chem.*, 1990, **396**, C35.
35 R. J. P. Corriu, Ph. Gerbier, C. Guérin, B. Henner, A. Jean and H. Mutin, *Organometallics*, 1992, **11**, 2507.
36 R. J. P. Corriu, Ph. Gerbier, C. Guérin, B. Henner and R. Fourcade, *J. Organomet. Chem.*, 1993, **449**, 111.
37 J.-L. Bréfort, R. J. P. Corriu, Ph. Gerbier, C. Guérin, B. Henner, A. Jean, Th. Kuhlmann, F. Garnier and A. Yassar, *Organometallics*, 1992, **11**, 2500.
38 G. Wegner, *Z. Naturforsh., Teil B*, 1968, **24**, 824.
39 R. Chance, R. H. Baughmann, H. Muller and C. J. Rockhardt, *J. Chem. Phys.*, 1977, **67**, 3616.
40 S. Kuroki, K. Okita, T. Kakigano, J. Ishikawa and M. Itoh, *Macromolecules*, 1998, **31**, 2804.
41 R. J. P. Corriu, Ph. Gerbier, C. Guérin and B. Henner, *Chem. Mater.*, 2000, **12**, 805.
42 G. T. Burns, R. B. Taylor, Y. Xu, A. Zangvil and G. Zank, *Chem. Mater.*, 1992, **4**, 1313.
43 P. Hsu, S. Ip, C. Park and M. McNallan, *J. Am. Ceram. Soc.*, 1993, **6**, 1621.
44 M. Itoh, K. Inoue, K. Iwata, J. Ishikawa and Y. Takenaka, *Adv. Mater.*, 1997, **9**, 1187.
45 G. Ramis, P. Quintard, M. Cauchetier, G. Busca and V. Lorenzelli, *J. Am. Ceram. Soc.*, 1989, **72**, 1692.
46 N. T. McDevitt and W. L. Baun, *Spectrochim. Acta*, 1964, **20**, 799.
47 E. G. Kendall, *Ceramics For Advanced Technologies*, eds. J. E. Hove and W. C. Riley, J. Wiley & Son, New York, 1965.
48 S. J. Gregg and K. S. W. Sing, *Adsorption, Surface Area and Porosity*, Academic Press, London, New York, 1982.
49 R. W. Chorley and P. W. Lednor, *Adv. Mater.*, 1991, **10**, 474.
50 L. M. Berger, *J. Hard Mater.*, 1992, **3**, 3.
51 R. J. P. Corriu, N. Devylder, C. Guèrin, B. Henner and A. Jean, *J. Organomet. Chem.*, 1996, **209**, 249.
52 S. Bourg, B. Boury and R. J. P. Corriu, *J. Mater. Chem.*, 1998, **8**, 1843.
53 T. C. Chou and J. Wadsworth, *J. Mater. Res.*, 1991, **6**, 796.
54 Y. Pan and J. L. Baptista, *J. Am. Ceram. Soc.*, 1996, **79**, 2017.
55 G. V. White, K. J. D. Mackenzie and J. H. Johnston, *J. Mater. Sci.*, 1992, **27**, 4287.
56 G. V. White, K. J. D. Mackenzie, I. W. Brown, M. E. Bowden and J. H. Johnston, *J. Mater. Sci.*, 1992, **27**, 4294.
57 G. V. White, K. J. D. Mackenzie, I. W. Brown and J. H. Johnston, *J. Mater. Sci.*, 1992, **27**, 4300.
58 K. Kamiga, T. Yoko and M. Bessho, *J. Mater. Sci.*, 1987, **22**, 937.
59 K. Ohno, *J. Mater. Sci.*, 1992, **27**, 658.
60 G. V. Samsonov, *Handbook of Physical Properties of Elements*, Plenum, New York, 1968.
61 SiC–4C were obtained from the pyrolysis of **1a** under argon at 1000 °C. The powders were thoroughly ground in an agate mortar prior to be fired.
62 R. Koc and J. S. Folmer, *J. Mater. Sci.*, 1997, **32**, 3101.